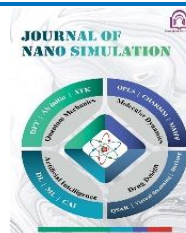




Damghan University Press



DFT study on interaction of triacetin with some chemical compounds in cigarette smoke

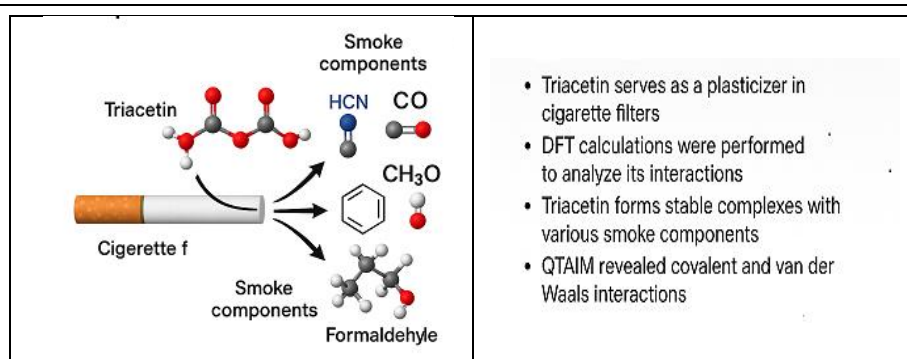
Abdol Hossein Masoudi Gazi*, Gholam Reza Moradi Robati

Chemistry Department of Tirtash Tobacco Research and Education center, Tirtash, Iran

HIGHLIGHTS

- Triacetin's molecular structure and interactions with cigarette smoke components were analyzed using Density Functional Theory (DFT).
- The strongest interaction was observed with hydrogen cyanide, while the weakest occurred with carbon monoxide.
- Adsorption was nonspontaneous ($\Delta G > 0$), with endothermic and exothermic interactions shaping triacetin's stability profile.
- NBO and QTAIM analyses revealed covalent and van der Waals interactions, with notable cage critical points and a dihydrogen bond.

GRAPHICAL ABSTRACT



ARTICLE INFO

Article history:

Received: 2025-04-06

Received in revised form: 2025-05-16

Accepted: 2025-05-24

Available online: 2025-06-23

Keywords:

Triacetin,
Density Functional Theory,
NBO,
QTAIM

ABSTRACT

Triacetin (1,3-Diacetyloxypropan-2-yl acetate) serves as a plasticizer in the manufacturing of cellulose acetate cigarette filters, composed of cellulose acetate fibers, plug wrap paper, hotmelt adhesive, and triacetin. Quantum chemical calculations and thermodynamic analyses were performed using Density Functional Theory (DFT) at the B3LYP level with the 6-311++G** basis set to examine triacetin's structure and its interactions with cigarette smoke chemical components. Results, corrected for intramolecular basis set superposition error (BSSE), revealed that bond formation primarily occurs through oxygen and hydrogen atoms. Among the studied complexes, triacetin exhibited the highest stability with hydrogen cyanide and the lowest stability with carbon monoxide, based on interaction energy values. All interactions showed nonspontaneous adsorption ($\Delta G > 0$), with positive ΔH values indicating endothermic behavior for triacetin-carbon monoxide and triacetin-benzene complexes, while other interactions were exothermic (negative ΔH). Natural Bond Orbital (NBO) analysis and Quantum Theory of Atoms in Molecules (QTAIM) demonstrated covalent characteristics for C-O, C-C, and C-H bonds in triacetin, alongside van der Waals interactions in its complexes. Notably, a unique cage critical point (CCP) was observed in the triacetin-formaldehyde complex, and a dihydrogen bond was identified in the triacetin-benzene interaction. These findings enhance our understanding of triacetin's behavior and interactions, contributing to the optimization of cigarette filter manufacturing.

*Email: a.h.masoudi51@gmail.com

1. Introduction

Triacetin, also known as 1,3-Diacetyloxypropan-2-yl acetate or glycerol triacetate, can be produced through the catalytic reaction of acetic acid or acetic anhydride with glycerol [1]. It is a colorless, oily liquid with a slightly fatty odor and a mild, sweet taste that becomes bitter at concentrations above 0.05%. Triacetin is soluble in both water and alcohol. One industrial method for utilizing glycerol is its acetylation with acetic acid. The products of this process have numerous industrial applications [2]. For instance, triacetate is used in the pharmaceutical and cosmetic industries, whereas monoacetate and diacetate are employed in the refrigeration industry and as raw materials for producing biodegradable polyesters [3,4].

Additionally, triacetate is utilized as a chemical additive in biodiesel, where it enhances the cetane number to reduce nitrogen oxide emissions to acceptable levels. It also shows potential as a replacement for conventional fuel additives [4,5]. Incorporating 10% (w/w) triacetate into biodiesel can improve its performance compared to pure biodiesel [6]. Biodiesel is a non-toxic, renewable, biodegradable, and safe fuel derived from natural sources such as vegetable oils, waste cooking oil, animal fat, and algae. It can be blended with diesel and used in diesel-powered vehicles. The positive impact of biodiesel on reducing air pollution has been confirmed by reputable global organizations [7]. Biodiesel is produced by combining long-chain monoalkyl esters of fatty acids, which result from the reaction of alcohol with renewable lipid materials [8,9].

Triacetate is primarily used as a plasticizer and gelatinizing agent in polymers and explosives, as well as an additive in tobacco, pharmaceutical formulations, and cosmetics [10]. Glycerol can be utilized to manufacture various additives, specialty chemicals, and pharmaceuticals, as well as fuels and polyesters for bakery products, ice cream, tobacco, lotions, and alkyd resins. It is also employed as an emulsifier, softening agent, stabilizer, wetting agent, and cosmetic ingredient. Triacetin, specifically, is used to stiffen cellulose acetate fibers in the production of cigarette filters. With a constant water content, cigarette filters stiffen within a few hours. Cigarette and filter manufacturers are fully aware that the plasticizer content in filters significantly affects their quality. Triacetin was identified as a plasticizer for cigarette filters [11]. A cigarette filter typically comprises cellulose acetate fibers, plug wrap paper, hotmelt adhesive, and triacetin [12]. Triacetin is commonly used as a plasticizer in the production of cellulose acetate filters and is a key component in cigarette filter manufacturing. To ensure sufficient stiffness, the Triacetin content in filters generally ranges between 6% and 9% of the total filter weight. Additionally, environmental factors such as temperature and relative humidity play a critical role in filter production. Monitoring Triacetin levels during manufacturing is essential to prevent soft or weak Triacetin injection. Furthermore, Triacetin is known to transfer into mainstream smoke and contribute to tar [13-15].

Computational chemistry numerically simulates chemical structures and reactions based on fundamental physical laws, specifically those governing the behavior of microscopic particles like electrons and nuclei [16,17]. In DFT, also referred to as Hohenberg-Kohn theory, the energy and electronic properties of a system in its ground state are calculated using electronic probability density. This theory establishes a one-to-one relationship between the ground-state electron density of a system and its energy, along with other properties. The primary objective of DFT is to provide suitable functions that relate electron density to system energy. DFT calculations begin by evaluating electronic probability density and determining the correlation energy with a reduced computational volume compared to other methods. B3LYP is considered the most prominent DFT method [18]. In this paper, the structures of triacetin and its complexes with chemical compounds found in cigarette smoke including carbon monoxide, acetone, formaldehyde, hydrogen cyanide, benzene, nicotine, and menthol have been optimized, and their bonding properties, structural parameters, and vibrational frequencies have been calculated. Subsequently, using NBO calculations, their atomic charges and second-order perturbation energies have been determined [19]. Finally, the energies resulting from the interactions and their relative stabilities have

been calculated. The details of these calculations and the obtained results are presented in the following sections.

2- Computational methods

In the present study, the structures of triacetin and its complexes resulting from the interactions of triacetin with the main chemical compounds in cigarette smoke, including carbon monoxide, hydrogen cyanide, formaldehyde, acetone, benzene, nicotine, and menthol were initially drawn using the Hyperchem 7.0 program. Subsequently, these structures were re-entered into the Gauss View 5.0 program [20] for optimization calculations and to obtain the minimum energy of the compounds. The optimization and frequency calculations were performed using DFT with the B3LYP functional [21] and the 6-311++G** basis set in the Gaussian 09 program [22], ensuring no imaginary frequencies were present for the structures of triacetin and its complexes.

Critical bond points, bond paths, and topological electron density analyses were conducted using the Quantum Theory of Atoms in Molecules (QTAIM) [23] with the aforementioned method and basis set, utilizing the AIM 2000 program [24]. These parameters serve as valuable indicators for evaluating the nature of bonds, such as covalent, van der Waals, hydrogen, and electrostatic interactions, while also quantitatively describing interatomic interactions. Additionally, NBO and charge transfer analyses were performed using the B3LYP functional and the 6-311++G** basis set with NBO software version 1.3 [19]. Further calculations were conducted to determine the HOMO, LUMO, and band gap energies, as well as to generate contours, electrostatic potential surfaces (ESPs), charge transfer electron densities, their energies, and natural atomic charges. In the present paper, the compound numbers of triacetin, triacetin-carbon monoxide complex, triacetin-hydrogen cyanide, triacetin-formaldehyde, triacetin-acetone, triacetin-benzene, triacetin-nicotine and triacetin-menthol are 1, 2, 3, 4, 5, 6, 7 and 8, respectively.

3- Results and Discussion

3-1- Energy Properties and Optimized Structures

In this study, geometric optimization calculations were performed to investigate the energy, structural, and electronic properties of the triacetin structure and its complexes. The calculations were conducted using DFT at the B3LYP level with the 6-311++G** basis set. The total electronic and interaction energies for triacetin and the adsorbed compounds were determined using the following equations:

$$\Delta E_{\text{int}} = E_{\text{(Complex)}} - \sum^E [E_{\text{(Triacetin)}} + E_{\text{(adsorbent)}}] \quad (1)$$

$$\Delta E_{\text{int}}^{\text{CP}} = \text{BSSE} + \Delta \text{ZPVE} + E_{\text{(Complex)}} - \sum^E [E_{\text{(Triacetin)}} + E_{\text{(adsorbed compound)}}] \quad (2)$$

The interaction energies are corrected by incorporating the intramolecular basis set superposition error (BSSE) and the zero-point vibrational energy (ΔZPVE) [25]. BSSE accounts for basis set superposition errors, while ΔZPVE reflects the vibrational energy of a molecule at absolute zero (0 K). Applying these corrections significantly impacts the $\Delta E_{\text{binding}}$ value. BSSE also addresses key errors in calculating the interaction energy for both weak van der Waals forces and strong covalent bonds in complexes [26, 27].

Table 1 summarizes the total electronic energy (E_{Total}), uncorrected interaction energy (ΔE_{int}), BSSE- and ΔZPVE -corrected interaction energy, and dipole moment. Among the adsorbed compounds, the one with the most negative energy is identified as the most stable. This indicates that structures with more negative energy are more stable on the complex surface. The complexes with the highest negative energy are more stable. Consequently, the calculations for the interaction energy (ΔE_{int}) of the structures in Table 1 indicate that the triacetin-hydrogen cyanide compound has the lowest interaction energy of -257.5 kcal/mol, making it more stable than the other six complexes due to the formation of stronger bonds and a more stable molecular equilibrium state. In contrast, the triacetin-carbon monoxide

Table 1 Total electronic energy E_{Total} , interaction energy ΔE_{int} , basis set superposition error (BSSE) and dipole moment for the optimized structure of triacetin and its complexes with seven chemical compounds present in mainstream cigarette smoke in the gas phase

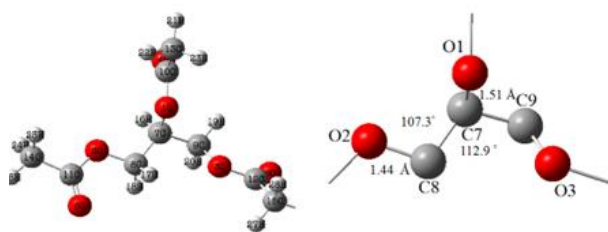
Compound	Property					Dipole moment (Debye)
	E_{Total} (Hartree)	ΔE_{int} (kcal.mol ⁻¹)	BSSE (kcal.mol ⁻¹)	$\Delta ZPVE$ (kcal.mol ⁻¹)	$\Delta E_{\text{int}}^{\text{CP}}$ (kcal.mol ⁻¹)	
Triacetin	-	-	-	-	-	2.756
Triacetin/Carbon monoxide	-916.369	-0.252	0.113	0.314	0.175	1.276
Triacetin/Hydrogen cyanide	-896.482	-5.257	0.231	0.927	-4.099	5.194
Triacetin/Formaldehyde	-917.566	-2.834	0.326	0.810	-1.697	4.046
Triacetin/Acetone	-996.242	-3.083	0.398	0.664	-2.020	4.835
Triacetin/Benzene	-1035.332	-1.247	0.383	0.563	-0.301	1.401
Triacetin/Nicotine	-1302.137	-1.741	0.214	0.625	-0.901	3.970
Triacetin/Menthol	-1271.506	-1.891	0.268	0.819	-0.803	2.728

Table 2 Thermodynamic parameters Enthalpy (ΔH), Gibbs Free Energy (ΔG), and Entropy (ΔS) for the optimized structure of triacetin and its complexes with seven chemical compounds present in mainstream cigarette smoke in the gas phase

Compound	Property		
	ΔH (kcal.mol ⁻¹)	ΔG (kcal.mol ⁻¹)	ΔS (kcal.mol ⁻¹ K ⁻¹)
Triacetin/Carbon monoxide	0.674	4.241	-0.011
Triacetin/Hydrogen cyanide	-4.144	3.217	-0.024
Triacetin/Formaldehyde	-1.436	6.143	-0.025
Triacetin/Acetone	-1.184	5.267	-0.021
Triacetin/Benzene	0.084	8.219	-0.027
Triacetin/Nicotine	-0.348	8.494	-0.029
Triacetin/Menthol	-0.443	8.827	-0.031

compound has the highest interaction energy of -252.0 kcal/mol, rendering it less stable than the other complexes.

By comparing the interaction energies of the seven optimized complexes in Table 1, their stability ranking is as follows: 3 > 5 > 4 > 8 > 7 > 6 > 2. Additionally, the interaction energy with BSSE correction is significantly reduced, by 9 to 20 percent, compared to the interaction energy without BSSE correction. Table 1 shows the interaction energy values with BSSE correction, highlighting their increase compared to the interaction energy without BSSE. Figures 1 and 2 illustrate the optimized geometric structures of triacetin and its complexes with cigarette smoke chemical compounds in the gas phase, calculated at the B3LYP/6-311++G** level.

**Figure 1** The most stable optimized geometric structure of triacetin in the gas phase using the B3LYP/6-311++G** method.

The dipole moment reflects the polarizability of the compounds. Based on the dipole moment calculations in Table 1, the triacetin-hydrogen cyanide

compound has the highest value of 194.5 Debye, indicating the highest polarizability. In contrast, the triacetin-carbon monoxide structure has the lowest dipole moment of 1.276 Debye, signifying the lowest polarizability. By comparing the dipole moments, the polarizability ranking of the structures in Table 1 is 3 > 5 > 4 > 7 > 8 > 6 > 2. The higher polarization values observed in the triacetin complexes are likely attributed to variations in charge distribution across the structures.

Calculations of Gibbs free energy (ΔG), enthalpy (ΔH), and entropy (ΔS) for the combination of triacetin and its complexes with cigarette smoke chemical compounds are derived using the following equations:

$$\Delta G = G_{(\text{complex})} - G_{(\text{Triacetin})} - G_{(\text{absorbent})} \quad (3)$$

$$\Delta H = H_{(\text{complex})} - H_{(\text{Triacetin})} - H_{(\text{absorbent})} \quad (4)$$

$$\Delta S = (\Delta H - \Delta G)/T \quad (5)$$

The results in Table 2 indicate that the ΔH values for triacetin-carbon monoxide and triacetin-benzene are positive, signifying endothermic interactions, while negative ΔH values for triacetin-hydrogen cyanide, triacetin-formaldehyde, triacetin-nicotine, and triacetin-menthol suggest exothermic interactions. The ΔH changes range from -144.4 kcal/mol to 0.674 kcal/mol. For all triacetin complexes with cigarette smoke components, $\Delta G > 0$ indicates non-spontaneous behavior. The triacetin-hydrogen cyanide complex, as the most stable structure, exhibits the lowest ΔG value, with ΔG

Table 3 NBO calculations, electron transfers, and second-order disorder energy (E^2), Non-diagonal Fock matrix for (F_{ij}), Energy difference ($\Delta\epsilon_{ij}$) optimized triacetin complexes in the gas phase

Compound	Lewis type NBO		Non Lewis type NBO		F_{ij} (a.u)	Charge Transfer
	Donor NBO(i)	Acceptor NBO (j)	E^2 (kcal.mol ⁻¹)	$\sum E^2$ (kcal.mol ⁻¹)		
Triacetin/Carbon monoxide	LP(1)O ₃₀	BD*(1) C ₁₃ - H ₂	0.06	0.06	0.007	0.00006
	LP(1)O ₆	BD*(1) C ₃₀ - H ₃₁	5.23		0.069	0.0070
	LP(2)O ₆	BD*(1) C ₃₀ - H ₃₁	2.70	7.93	0.041	0.0063
Triacetin/Hydrogen cyanide	LP(1)O ₄	BD*(1) H ₃₀ - C ₃₁	1.00		0.030	0.0015
	LP(2)O ₄	BD*(1) H ₃₀ - C ₃₁	0.13		0.005	0.1250
	LP(1)O ₃₃	BD*(1) C ₁₄ - H ₂₅	0.30	1.53	0.017	0.0005
	LP(2)O ₃₃	BD*(2) O ₅ - C ₁₁	0.1		0.005	0.0049
Triacetin/Formaldehyde	LP(1)O ₃₃	BD*(1) C ₁₅ - H ₂₇	0.82		0.027	0.0011
	LP(2)O ₃₃	BD*(1) C ₁₅ - H ₂₇	0.55	1.37	0.018	0.0013
	LP(1)O ₃	BD*(1) C ₃₄ - H ₄₀	0.28		0.015	0.0004
Triacetin/Benzene	LP(1)O ₅	BD*(1) C ₃₃ - H ₃₉	0.47		0.021	0.0006
	LP(2)O ₅	BD*(1) C ₃₃ - H ₃₉	0.29	1.04	0.014	0.0006
	LP(1)O ₅	BD*(1) C ₃₉ - H ₄₈	0.12		0.011	0.0001
	LP(2)O ₅	BD*(1) C ₃₉ - H ₄₈	0.27		0.013	0.0006
Triacetin/Nicotine	LP(2)O ₅	BD*(1) C ₄₁ - H ₅₂	0.12	1.39	0.008	0.0002
	LP(1)N ₄₀	BD*(1) C ₁₄ - H ₂₆	0.88		0.023	0.0010
	LP(1)O ₃₀	BD*(1) C ₁₅ - H ₂₉	1.85	1.85	0.039	0.0028

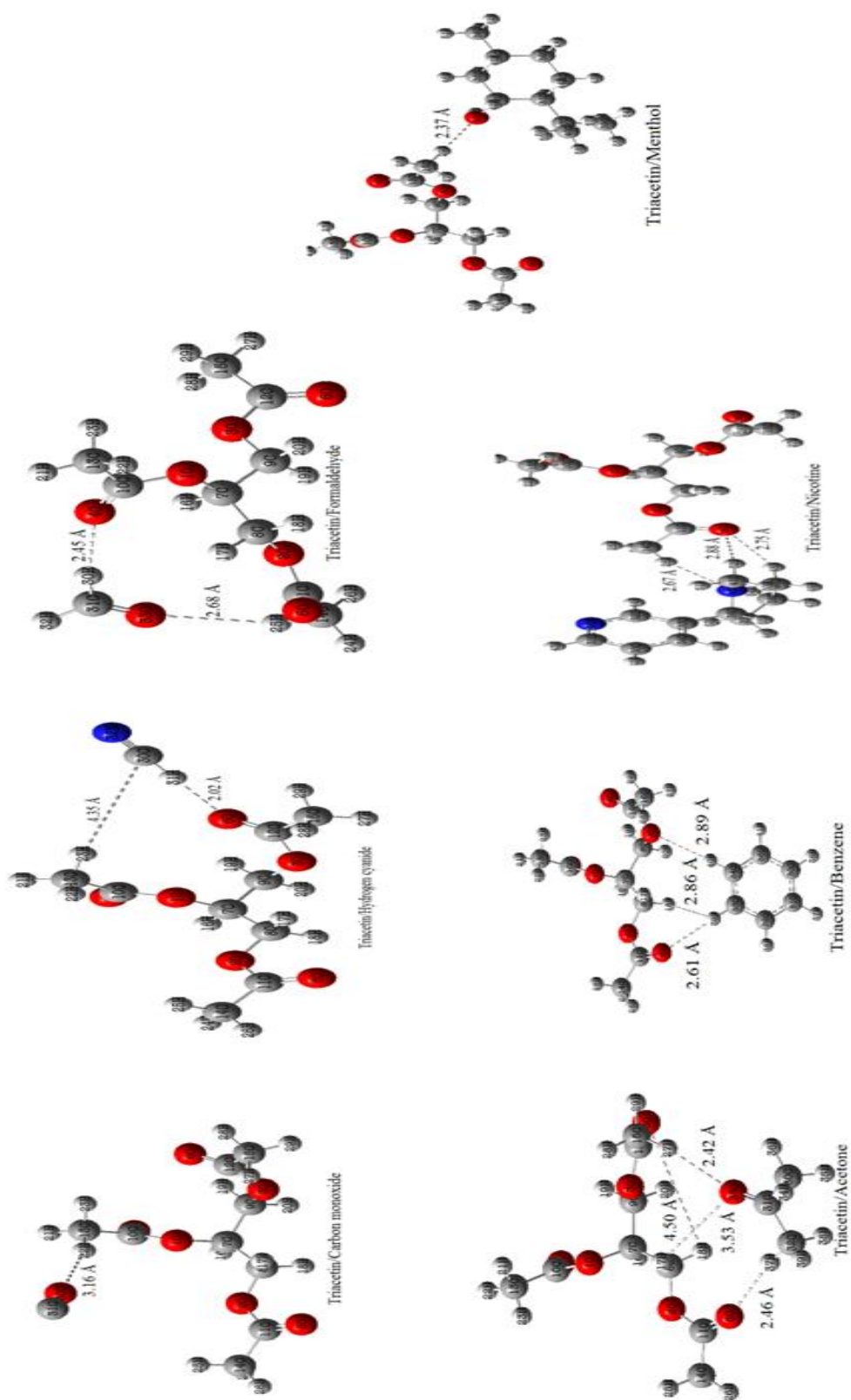


Figure 2 Optimized geometric structures of triacetin complexes with cigarette smoke

changes ranging from 217.3 kcal/mol to 827.8 kcal/mol. Additionally, negative ΔS values for all complexes suggest reduced system entropy during the adsorption process. The changes in ΔS range from -0.031 kcal/mol-K to -0.011 kcal/mol-K. All triacetin complexes exhibit physical adsorption, driven by intermolecular van der Waals forces, as confirmed by QTAIM analysis.

Some bond lengths, angles, and dihedral angles for the optimized structures of triacetin and its complexes are presented in Table S1. The results indicate that bond lengths and angles, such as C13-H22, C13-C10, C10=O4, C10-O1, C7-C8-O2, O2-C11-O5, O3-C9-C7, and C9-C7-C8, show no significant changes. This suggests that the bond lengths of the complexes and products are primarily determined by the nature of the covalently bonded atoms, meaning physical adsorption of the starting material has minimal impact on bond lengths.

The bond lengths of the optimized triacetin structure and their averages during complex formation when interacting with cigarette smoke components are as follows: C13-H22 (1.092 Å, 1.090 Å), C13-C10 (1.505 Å, 1.504 Å), C10=O4 (1.206 Å, 1.205 Å), and C10-O1 (1.357 Å, 1.358 Å). Similarly, bond angles such as C7-C8-O2 (32.107°, 28.107°), O2-C11-O5 (14.123°, 07.123°), O3-C9-C7 (70.108°, 96.109°), and C9-C7-C8 (98.112°, 79.112°) are very similar and closely aligned. For all complexes of triacetin with cigarette smoke chemical compounds, the bond length of the adsorbed starting material after complex formation is longer than its value in the single state, indicating physical adsorption on the compound's surface. The shortest bond length between the interacting compounds reflects a stronger bond, creating the strongest interaction during adsorption on the surface. Figure 2 illustrates the intermolecular and intramolecular interactions of triacetin complexes with cigarette smoke components. The shortest intermolecular bond length, O6-H31, is 2.02 Å and belongs to the most stable optimized triacetin-hydrogen cyanide complex. This strong bond facilitates the most significant interaction for hydrogen cyanide adsorption onto the triacetin structure.

The natural atomic charges [28] for the optimized triacetin structure and its interactions with the main chemical constituents of cigarette smoke are calculated and presented in Table S2. Hydrogen atoms (H18, H22, H25, H27) and C11 carry positive charges, while carbon (C14, C13) and oxygen (O5, O6) atoms carry negative charges. For instance, in the most stable triacetin-hydrogen cyanide complex, all hydrogen atoms have positive charges. The atomic charges of C13, O6, and H22 are -0.668, -0.636, and 0.227, respectively. In the single state of triacetin, the charges of these atoms are -0.667, -0.591, and 0.230. This lack of change in charge signs during the interaction indicates a physical interaction between triacetin and hydrogen cyanide. Similarly, no significant changes are observed in the atomic charges of the triacetin compound in comparison to the complex.

3.2. NBO analysis

The distribution of electrons in atomic and molecular orbitals forms the basis for calculating atomic charges and molecular bonds. NBO analysis highlights the interactions between intermolecular orbitals within the complex, emphasizing charge transfer [29]. All possible interactions between filled Lewis-type NBOs (donors) and empty non-Lewis-type NBOs (acceptors) are analyzed, and their energies are calculated using perturbation theory. For each donor i and acceptor j NBO, the stability energy E corresponding to the $i \rightarrow j$ or $\sigma \rightarrow \sigma^*$ interaction is determined by the following equation.

$$\Delta E_{i \rightarrow j} = q_i \frac{F_{(ij)}^2}{\epsilon_j - \epsilon_i} \quad (6)$$

Where q_i represents the occupancy number of the i -th donor orbital, ϵ_i and ϵ_j are the diagonal elements (orbital energies), and $F_{(ij)}$ denotes the off-diagonal elements of the NBO Fock matrix. The transferred charges $q(n \rightarrow \sigma^*)$ and $q(\pi \rightarrow \sigma^*)$ for the complexes are calculated using the following equation [30,31].

$$q = -2(F_{(i,j)}/E_j - E_i)^2 \quad (7)$$

Table 3 presents the stability energy, charge transfer, $F_{(i,j)}$ (non-diagonal elements of the Fock matrix), and the energy difference $\Delta \epsilon$ between the electron donor (i) and acceptor (j) for key intermolecular interactions in the

most stable optimized structure of triacetin and its complexes with major chemical components of cigarette smoke. The calculated energies are reported in atomic units (a.u.), while the second-order perturbation energy is expressed in kcal-mol⁻¹. According to the data in Table 3, in most compounds, the antibonding orbitals (electron acceptors) interact with the electron pairs on O6, O5, O4, and O3 of the triacetin structure, as well as O30, O33, and N40 of cigarette smoke chemical compounds (electron donors). Specifically, stability energy calculations $E^{(2)}$ for the triacetin-hydrogen cyanide and triacetin-benzene complexes result from interactions between the antibonding orbitals of hydrogen cyanide and benzene with the O6, O5, and O3 electron pairs of triacetin. Similarly, for the triacetin-carbon monoxide, triacetin-acetone, and triacetin-menthol complexes, the antibonding orbitals of triacetin interact with the O30 and O33 electron pairs of carbon monoxide, acetone, and menthol.

For the triacetin-formaldehyde complex, the interaction involves antibonding orbitals from two forms of the triacetin structure with the O33 electron pair of formaldehyde, as well as antibonding orbitals of formaldehyde with the O4 electron pair of triacetin. Similarly, in the triacetin-nicotine complex, antibonding orbitals from two forms of the triacetin structure interact with the N40 electron pair of nicotine, while the antibonding orbitals of nicotine interact with the O5 electron pair of triacetin. The total stability energy $E^{(2)}$ for the optimized structures of triacetin and its complexes including triacetin-carbon monoxide, triacetin-hydrogen cyanide, triacetin-formaldehyde, triacetin-acetone, triacetin-benzene, triacetin-nicotine, and triacetin-menthol are 233.7, 232.4, 242.0, 233.8, 235.6, 233.2, 235.4, and 232.7 kcal/mol, respectively.

The triacetin-hydrogen cyanide complex exhibits the highest total stability energy $E^{(2)}$, indicating a strong interaction between the electron donor and acceptor. This is attributed to the effective interaction of LP(1)O6 in the triacetin structure with the $BD^*(1)$ antibonding orbital of the C30-H31 bond in hydrogen cyanide. Additionally, LP(2)O6 interacts with the $BD^*(1)$ antibonding orbital of the C30-H31 bond, showing that the electron donor orbital (triacetin) has a greater tendency to transfer electrons to the electron acceptor (hydrogen cyanide). For this reason, this complex is more stable than the other complexes. The results from NBO analysis align with the interaction energies in Table 1. Additionally, NBO calculations indicate that the stability energy of effective interactions for the most stable triacetin-hydrogen cyanide complex is the highest among all complexes, confirming a strong interaction between the electron donor and acceptor.

3.3 Quantum mechanical descriptors for the structure of triacetin and its complexes

The energy difference between the highest occupied molecular orbital (HOMO) and the lowest unoccupied molecular orbital (LUMO), known as the energy gap (E_g), serves as a measure of electronic conductivity [32]. To describe the electronic properties of compounds and predict their chemical behavior, quantum mechanical descriptors are employed, including electron chemical potential (μ), electronegativity (χ), Electrophilicity index (ω), hardness index (η), softness index (S), energy gap (E_g), maximum electron charge (ΔN), and formation energy (E_f). The chemical potential is calculated using Koopman's theorem from the following equation [33,34]:

$$\mu = -(I + A)/2 \quad (8)$$

$$\mu = (E_{HOMO} + E_{LUMO})/2 \quad (9)$$

Where I ($-E_{HOMO}$) and A ($-E_{LUMO}$) represent the ionization and electronegativity potential energies of the structures, respectively. The hardness index, which measures the resistance of a chemical species to changes in its electronic structure, is calculated using the following equation:

$$\eta = (I - A)/2 \quad (10)$$

$$\eta = \frac{E_{LUMO} - E_{HOMO}}{2} \quad (11)$$

The electrophilicity index (ω) is defined by Parr [34] using the following equation:

$$\omega = \mu^2/2\eta \quad (12)$$

Quantum parameters such as electronegativity (χ), softness index (S), energy gap, maximum electric charge (ΔN), and Fermi energy (E_F) of compounds [35,36] are calculated using the following equations:

$$\chi = -\mu \quad (13)$$

$$S = 1/2\eta \quad (14)$$

$$E_g = E_{LUMO} - E_{HOMO} \quad (15)$$

$$\Delta N = -\mu/\eta \quad (16)$$

$$E_F = E_{HOMO} + (E_{LUMO} - E_{HOMO})/2 \quad (17)$$

Calculations of quantum mechanical descriptors for the triacetin structure and its complexes, shown in Table 4, describe their electronic properties and

predict their chemical behaviors. A comparison of the energy gaps reveals that, after complex formation, the energy gap of triacetin complexes decreases compared to the standalone triacetin structure, indicating easier charge transfer. The highest energy gap (7.15 eV) is observed in the triacetin-hydrogen cyanide complex, which closely matches the energy gap of the triacetin structure, reflecting the interaction between the two structures. In contrast, the lowest energy gap (5.21 eV) is found in the triacetin-nicotine complex, suggesting that this compound facilitates electron transfer most readily. The energy gap values for triacetin complexes range from 7.15 to 5.21 eV. The hardness index (η) and chemical potential (μ) are key indicators of

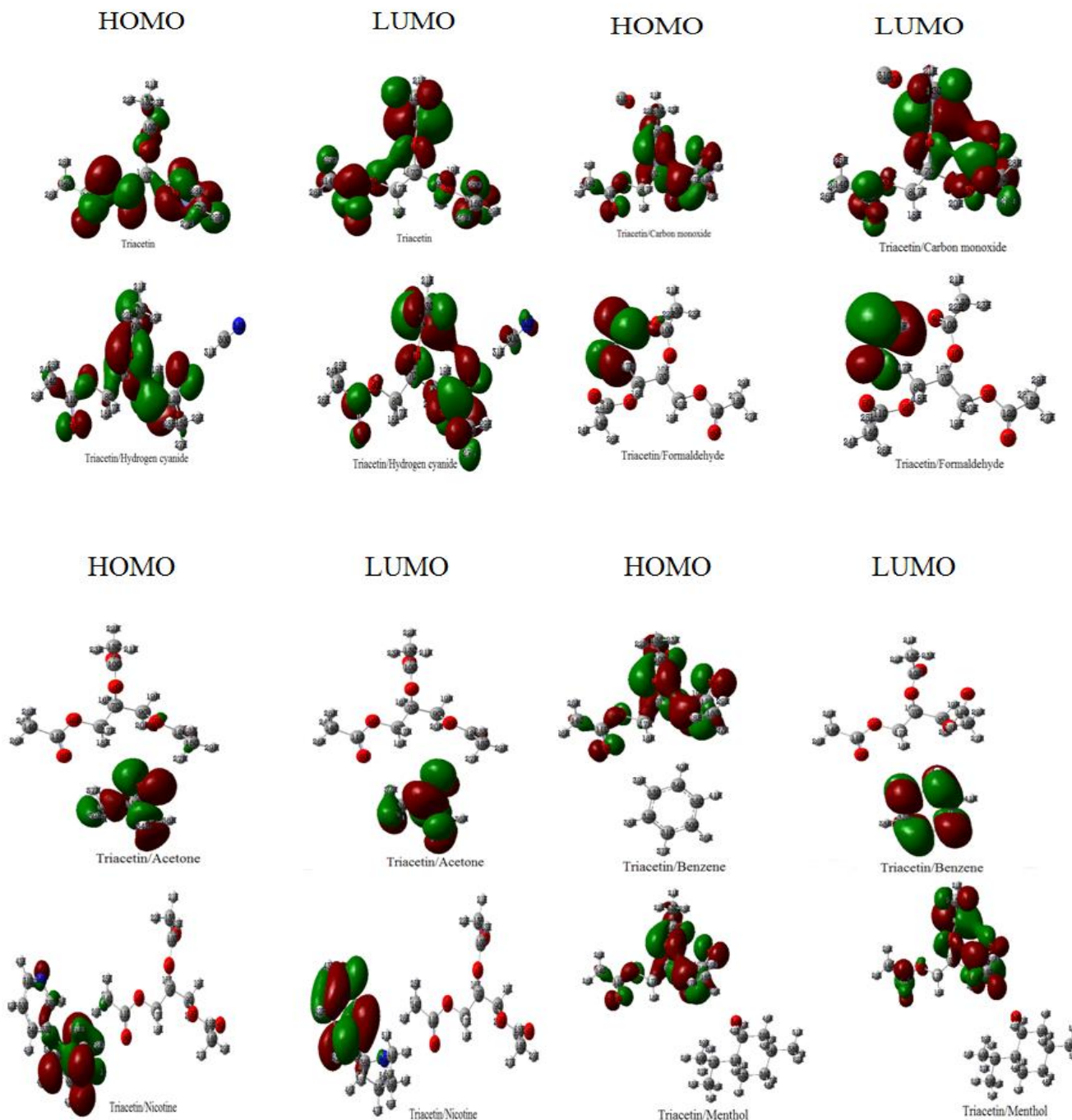


Figure 3 HOMO and LUMO frontier molecular orbitals of triacetin and its complex with cigarette smoke chemical compounds

molecular stability and reactivity. The highest chemical potential (-3.60-3.60 eV) is observed in the triacetin-nicotine complex, while the lowest (-4.56-4.56 eV) is seen in the triacetin-carbon monoxide complex, indicating the latter has higher reactivity compared to the other complexes.

The chemical potential values for triacetin complexes range from -3.60 to -4.56 electron-volts. According to Table 4, the interaction of cigarette smoke chemical compounds with the triacetin structure reduces the hardness index (η) of the complexes, indicating decreased stability and increased reactivity. The highest hardness index (η) is observed in the triacetin-hydrogen cyanide complex (3.57 eV), while the lowest is in the triacetin-nicotine complex (2.60 eV), suggesting that the latter has greater reactivity.

The highest electrophilicity index (ω) is associated with the triacetin-formaldehyde complex (3.47 eV), indicating its high electrophilic nature, while the lowest (ω) is seen in the triacetin-benzene complex (2.14 eV). The highest electronegativity index (χ) is found in the triacetin-carbon monoxide complex (4.56 eV), and the lowest in the triacetin-nicotine complex (3.60 eV), with all complexes showing closely aligned electronegativity values. The softness index (S) for all triacetin complexes is similar, ranging between 0.19 and 0.13 eV. Negative values of the maximum electric charge (ΔN) indicate charge transfer from cigarette smoke compounds to the triacetin structure, while positive values reflect charge transfer from triacetin to cigarette smoke compounds.

In Table 4, all calculated ΔN values for triacetin complexes are positive. The chemical potential values for triacetin complexes range from -3.60 to -4.56 electron-volts. According to Table 4, the interaction of cigarette smoke chemical compounds with the triacetin structure reduces the hardness index (η) of the complexes, indicating decreased stability and increased reactivity. The highest hardness index (η) is observed in the triacetin-hydrogen cyanide complex (3.57 eV), while the lowest is in the triacetin-nicotine complex (2.60 eV), suggesting that the latter has greater reactivity.

The highest electrophilicity index (ω) is associated with the triacetin-formaldehyde complex (3.47 eV), indicating its high electrophilic nature, while the lowest (ω) is seen in the triacetin-benzene complex (2.14 eV). The highest electronegativity index (χ) is found in the triacetin-carbon monoxide complex (4.56 eV), and the lowest in the triacetin-nicotine complex (3.60 eV), with all complexes showing closely aligned electronegativity values.

The softness index (S) for all triacetin complexes is similar, ranging between 0.19 and 0.13 eV. Negative values of the maximum electric charge (ΔN) indicate charge transfer from cigarette smoke compounds to the triacetin structure, while positive values reflect charge transfer from triacetin to cigarette smoke compounds. In Table 4, all calculated ΔN values for triacetin complexes are positive.

The chemical potential values for triacetin complexes range from -3.60 to -4.56 electron-volts. According to Table 4, the interaction of cigarette smoke chemical compounds with the triacetin structure reduces the hardness index (η) of the complexes, indicating decreased stability and increased reactivity. The highest hardness index (η) is observed in the triacetin-hydrogen cyanide complex (3.57 eV), while the lowest is in the triacetin-nicotine complex (2.60 eV), suggesting that the latter has greater reactivity. The highest electrophilicity index (ω) is associated with the triacetin-formaldehyde complex (3.47 eV), indicating its high electrophilic nature, while the lowest (ω) is seen in the triacetin-benzene complex (2.14 eV).

The highest electronegativity index (χ) is found in the triacetin-carbon monoxide complex (4.56 eV), and the lowest in the triacetin-nicotine complex (3.60 eV), with all complexes showing closely aligned electronegativity values. The softness index (S) for all triacetin complexes is similar, ranging between 0.19 and 0.13 eV. Negative values of the maximum electric charge (ΔN) indicate charge compounds. In Table 4, all calculated ΔN values for triacetin complexes are positive.

The frontier molecular orbitals of the triacetin structure and its complexes with cigarette smoke chemical compounds are illustrated in Figure 3. In this figure, the red and green regions represent the negative and positive areas of the wave functions for the HOMO and LUMO orbitals, respectively. The HOMO (highest occupied molecular orbital) and LUMO (lowest unoccupied molecular orbital) in the triacetin structure are distributed almost

symmetrically. Upon interaction with cigarette smoke chemical compounds, the HOMO and LUMO orbitals for the triacetin-carbon monoxide and triacetin-menthol complexes remain localized on the triacetin structure. In the triacetin-hydrogen cyanide complex, the HOMO orbitals are confined to the triacetin structure, while the LUMO orbitals are predominantly located on the triacetin structure and partially on the hydrogen cyanide molecule. For the triacetin-formaldehyde, triacetin-acetone, and triacetin-nicotine complexes, both the HOMO and LUMO orbitals are concentrated on formaldehyde, acetone, and nicotine, respectively. In the case of the triacetin-benzene complex, the HOMO orbitals are situated on the triacetin structure, whereas the LUMO orbitals are primarily distributed across the benzene molecule.

transfer from cigarette smoke compounds to the triacetin structure, while positive values reflect charge transfer from triacetin to cigarette smoke. The density of states (DOS) for the triacetin structure and its complexes with cigarette smoke compounds is illustrated in Figure 4.

The DOS diagram is essential for visualizing molecular orbitals and their roles in chemical bonding. It also helps distinguish the bonding, antibonding, and nonbonding nature of orbitals and their interactions.

In Figure 4 positive DOS values correspond to bonding interactions, negative values to antibonding interactions (depending on the population overlap), and zero values to nonbonding interactions. Green lines represent occupied orbitals, blue lines denote unoccupied orbitals, and the gap between them indicates the band gap. The triacetin-nicotine complex exhibits the shortest band gap (21.5 eV), facilitating charge transfer, while the triacetin-hydrogen cyanide complex has the longest band gap (15.7 eV), reflecting a less reactive state.

The electrostatic potential (ESP) levels for the triacetin structure and its complexes with cigarette smoke chemical compounds are depicted as contours in Figure 5. Contour maps illustrate the electron density distribution of a structure, with red and yellow regions representing the negative and positive areas of the wave functions, respectively. The charge distribution in the single-state triacetin structure is symmetrical. However, upon forming complexes with cigarette smoke chemical compounds, the charge distribution becomes asymmetrical. This is reflected in the dipole moment values, where the triacetin-hydrogen cyanide complex exhibits the highest asymmetry, with a dipole moment of 194.5 Debye, while the triacetin-carbon monoxide complex shows the lowest asymmetry, with a dipole moment of 1.276 Debye.

3.4 Quantum Theory of Atoms in Molecules (QTAIM) Analysis for Triacetin and Its Complexes

Quantum Theory of Atoms in Molecules (QTAIM) calculations for selected intra- and intermolecular bonds in the structure of Triacetin and its complexes are summarized in Tables 5 and 6. These calculations include Hessian eigenvalues ($\lambda_1, \lambda_2, \lambda_3$), electron density (ρ_b), Laplacian of electron density ($\nabla^2\rho_b$), kinetic energy density (G_b), electron potential (V_b), electron Hamiltonian (H_b), and bond ellipticity (ϵ) at the bond critical points (BCP). Figure 6 illustrates the topological structures of Triacetin and its complexes. In these figures, bond critical points, ring critical points, and cage critical points are represented by red, yellow, and green dots, respectively.

To better describe the properties of bond critical points (BCPs), parameters such as charge density (ρ), Laplacian ($\nabla^2\rho$), and bond ellipticity (ϵ) are utilized. The Laplacian $\nabla^2\rho$ can be expressed as $\nabla^2\rho = \lambda_1 + \lambda_2 + \lambda_3$, while bond ellipticity is defined as $\epsilon = \lambda_1 / \lambda_2 - 1$, and the electron Hamiltonian H_b is given by $H_b = G_b + V_b$. The bond ellipticity ϵ is always positive since $\lambda_1 < \lambda_2 < 0$. Generally, values of bond ellipticity smaller than 0.1 correspond to single covalent bonds, whereas those exceeding 0.1 indicate electrostatic or double bonds. Additionally, bond ellipticity values tend to be higher for weak interactions and lower for strong bonds with shorter bond lengths [37, 38].

critical bond points have eigenvalues and an algebraic sign sum of (3, -1). These bonds feature two negative eigenvalues ($\lambda_1 < \lambda_2 < 0$) and one positive eigenvalue ($\lambda_3 > 0$). The magnitude of the Hessian eigenvalues follows the

Table 5 Calculations of critical bond points and Hessian values by the QTAIM method in bond paths for the structure of triacetin and the complexes triacetin-carbon monoxide, triacetin-hydrogen cyanide, triacetin-formaldehyde. Hessian eigenvalues (λ_1 - λ_2 - λ_3), Bond ellipticity (ϵ), Electron density (ρ_b), Electron Laplacian ($\nabla^2\rho_b$), Electronic Hamiltonian (H_b), Kinetic energy (G_b), Electronic potential (V_b). (Values λ_1 , λ_2 , λ_3 and calculated energies are in (a.u))

Compound	Property											
	BCP	Bond	λ_1	λ_2	λ_3	ϵ	ρ_b	$\nabla^2\rho_b$	H_b	G_b	V_b	V_b/G_b
Triacetin	1	C7-C9	-0.5064	-0.4920	0.3746	0.0292	0.2557	-0.6236	-0.2107	0.0548	-0.2656	4.8467
	2	C7-O1	-0.4066	-0.3931	0.4166	0.0343	0.2355	-0.3828	-0.2949	0.1991	-0.4940	2.4811
	8	C7-H16	-0.7953	-0.7724	0.5712	0.0296	0.2867	-0.9964	-0.2837	0.0346	-0.3184	9.2023
Triacetin/Carbon monoxide	30	C31-O30	-1.6279	-1.6278	3.9055	0.00006	0.4873	0.6496	-0.8608	1.0232	-1.8840	1.8412
	29	H22-O30	-0.0013	-0.0013	0.0009	0.0076	0.0016	0.0068	0.0004	0.0013	-0.0009	0.6923
Triacetin/Hydrogen cyanide	13	C30-H23	-0.0002	-0.0002	0.0024	0.0400	0.0005	0.0016	0.0002	0.0003	-0.0001	0.3333
	30	H31-O6	-0.0126	-0.0121	0.0719	0.0413	0.0118	0.0468	0.0024	0.0093	-0.0069	0.7419
Triacetin/Formaldehyde	29	H30-O4	-0.0081	-0.0079	0.0440	0.0253	0.0085	0.0276	0.0009	0.0060	-0.0050	0.8333
	30	O33-H25	-0.0047	-0.0041	0.0279	0.1463	0.0054	0.0188	0.0007	0.0040	-0.0032	0.8000
	33	C31-O33	-1.0582	-1.0325	2.1579	0.0248	0.4090	0.0668	-0.6848	0.7016	-1.3865	1.9761

Table 6 Calculated critical bond points and Hessian values by the QTAIM method in bond paths for the complexes trystine-acetone, trystine-benzene, trystine-nicotine and trystine-menthol. (Values λ_1 , λ_2 , λ_3 and calculated energies are in (a.u))

Compound	Property											
	BCP	Bond	λ_1	λ_2	λ_3	ϵ	ρ_b	$\nabla^2\rho_b$	H_b	G_b	V_b	V_b/G_b
Triacetin/Acetone	32	O33-H27	-0.0133	-0.0129	0.0695	0.0310	0.0127	0.0432	0.0016	0.0091	-0.0075	0.8241
	17	O33-H17	-0.0058	-0.0057	0.0316	0.0175	0.0065	0.0200	0.0006	0.0043	-0.0037	0.8604
	36	O33-C31	-1.0020	-0.9719	1.8346	0.0309	0.3964	-0.1392	-0.6573	0.6224	-1.2797	2.0560
	5	H18-O6	-0.0072	-0.0066	0.0430	0.0909	0.0090	0.0288	0.0009	0.0063	-0.0054	0.8571
	27	H37-O5	-0.0132	-0.0127	0.0721	0.0393	0.0126	0.0460	0.0019	0.0096	-0.0076	0.7916
Triacetin/Benzene	24	H40-O3	-0.0031	-0.0030	0.0186	0.0333	0.0037	0.0124	0.0004	0.0026	-0.0021	0.8076
	32	H39-H18	-0.0015	-0.0002	0.0105	6.5000	0.0023	0.0084	0.0005	0.0016	-0.0011	0.6875
	18	H39-O5	-0.0055	-0.0054	0.0311	0.0185	0.0062	0.0200	0.0007	0.0043	-0.0036	0.8372
	41	C23-H39	-0.7630	-0.7507	0.5328	0.0163	0.2832	-0.9808	-0.2815	0.0363	-0.3179	8.7575
Triacetin/Nicotine	31	N40-H26	-0.0069	-0.0068	0.0335	0.0147	0.0079	0.0196	0.0005	0.0044	-0.0038	0.8636
	33	H52-O5	-0.0034	-0.0031	0.0201	0.0967	0.0041	0.0132	0.0005	0.0028	-0.0023	0.8214
	40	H48-O5	-0.0047	-0.0044	0.0258	0.0681	0.0054	0.0164	0.0005	0.0036	-0.0030	0.8333
Triacetin/Menthol	29	H29-O30	-0.0114	-0.0102	0.0569	0.1176	0.0108	0.0352	0.0012	0.0075	-0.0062	0.8266
	30	C32-O30	-0.4320	-0.4282	0.4198	0.0088	0.2436	-0.4404	-0.3095	0.1994	-0.5090	2.5526

order $\lambda_1 < \lambda_2 < \lambda_3$. Charge density (ρ) at bond critical points (BCPs) indicates bond strength and bond order. In Tables 5 and 6, for the optimized structure of triacetin and its complexes,

If ρ is large, $\nabla^2\rho < 0$, and $H_b < 0$, the interaction is shared, with charge concentrated in the internuclear region, characteristic of polar and covalent bonds. Conversely, if $\nabla^2\rho > 0$ and $H_b > 0$ with low ρ , the interaction exhibits van

der Waals characteristics and is considered weak. As ρ increases, the interaction becomes ionic (electrostatic).

Specifically, if $\rho_b < 0.1$ atomic units (a.u.) and $\nabla^2\rho$ is small and positive, the interaction is predominantly electrostatic. For $\rho_b > 0.1$ a.u. and $\nabla^2\rho$ negative, the interaction is covalent. If $\nabla^2\rho > 0$ and $H_b < 0$ (small, negative values), the interaction combines covalent and electrostatic features.

The parameter V_b/G_b is used to predict intermolecular interactions. If $V_b/G_b \geq 1$, the interaction is categorized as ionic, van der Waals, or electrostatic. When $1 < V_b/G_b < 2$, the interaction is considered intermediate, and for $V_b/G_b > 2$, the interaction is classified as covalent [39-41].

In Tables 5 and 6, as well as Figure 6, for the optimized structure of triacetin and its complexes, the intermolecular and intramolecular interactions are as follows:

For the triacetin structure, all critical bond points have $\nabla^2\rho > 0$ and $H_b < 0$, with $V_b/G_b > 2$ and bond ellipticity smaller than 0.1, indicating that all bonds exhibit

0. With the lowest charge density (ρ) among all bonds, $V_b/G_b \leq 1$, and bond ellipticity smaller than 0.1, this interaction is classified as van der Waals in nature, indicating a weak interaction.

In the triacetin-hydrogen cyanide complex, two intermolecular interactions involving the C30-H23 and H31-O6 bonds are observed, both having $\nabla^2\rho > 0$ and $H_b > 0$. Due to their low charge density (ρ), $V_b/G_b \leq 1$, and bond ellipticity smaller than 0.1, these interactions are also characterized as van der Waals and considered weak. The triacetin-formaldehyde complex exhibits two intermolecular interactions involving the H30-O4 and O33-H25 bonds. These interactions are characterized as van der Waals and considered weak due to having the lowest charge density (ρ) compared to other bonds.

The triacetin-acetone complex contains three intermolecular interactions (O33-H27, O33-H17, H37-O5) and one intramolecular interaction (H18-O6). All of these bonds have $\nabla^2\rho > 0$ and $H_b > 0$. With the lowest charge density (ρ), $V_b/G_b \leq 1$, and bond ellipticity smaller than 0.1, these interactions are classified as van der Waals and considered weak. The triacetin-benzene complex exhibits three intermolecular interactions involving the H40-O3,

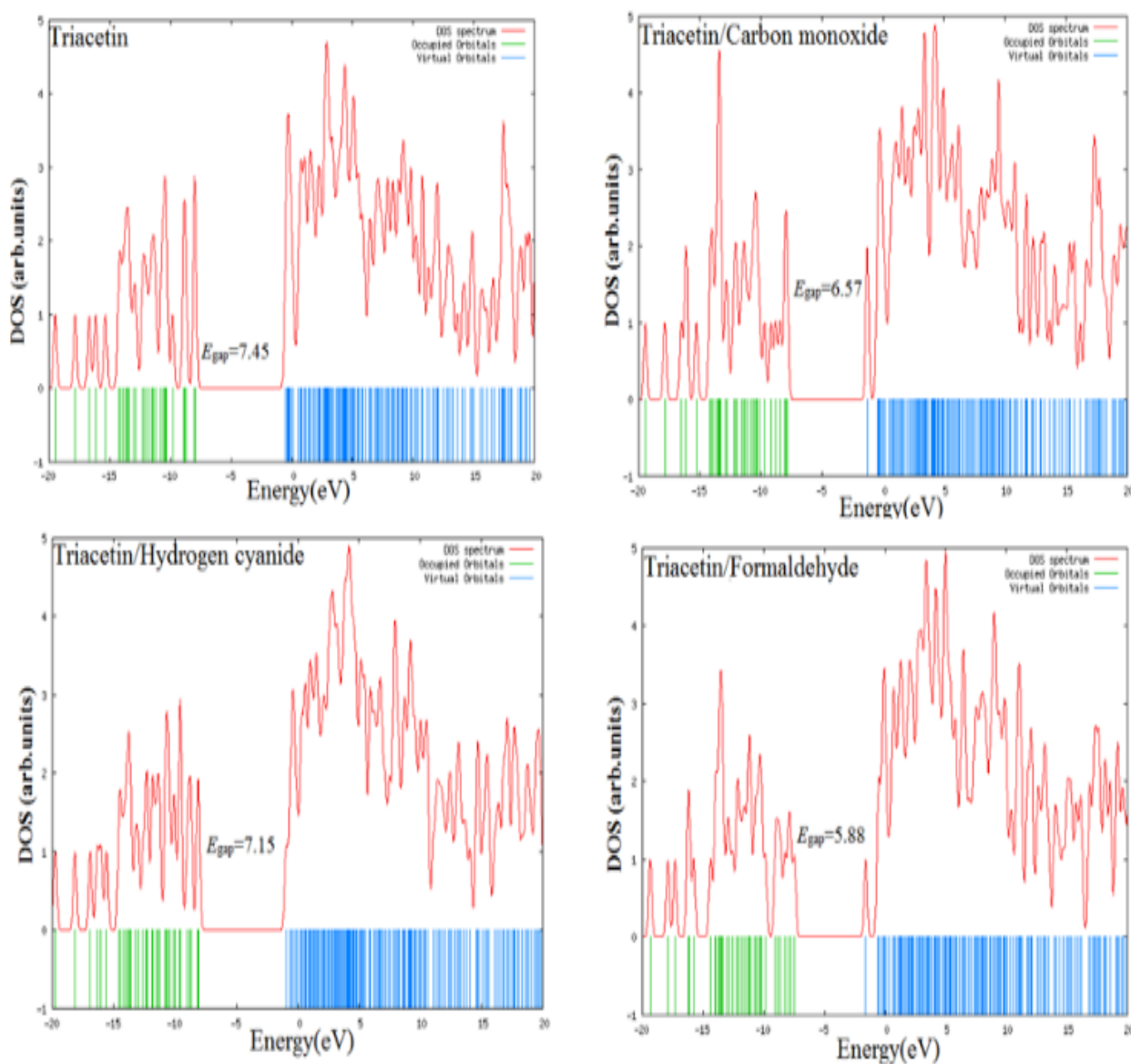


Figure 4 DOS diagram of triacetin compound and its complexes with cigarette smoke chemical compounds in the gas phase.

covalent character. In the triacetin-carbon monoxide complex, the intermolecular interaction related to the H22-O30 bond has $\nabla^2\rho > 0$ and $H_b >$

H39-O5, and H39-H18 bonds. For all three, $\nabla^2\rho > 0$ and $H_b > 0$, while the charge density (ρ) is the lowest among the bonds.

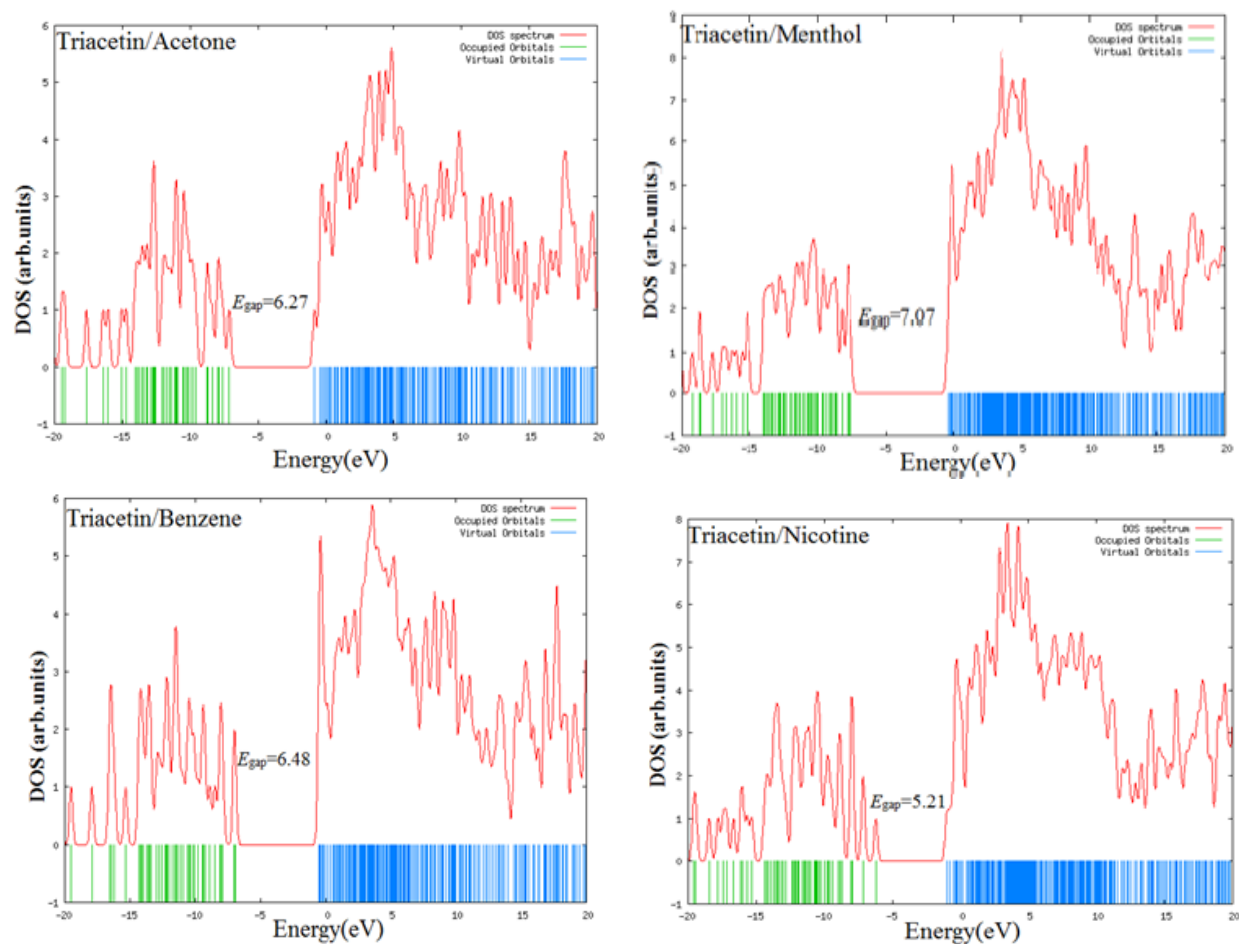


Figure 4 continued

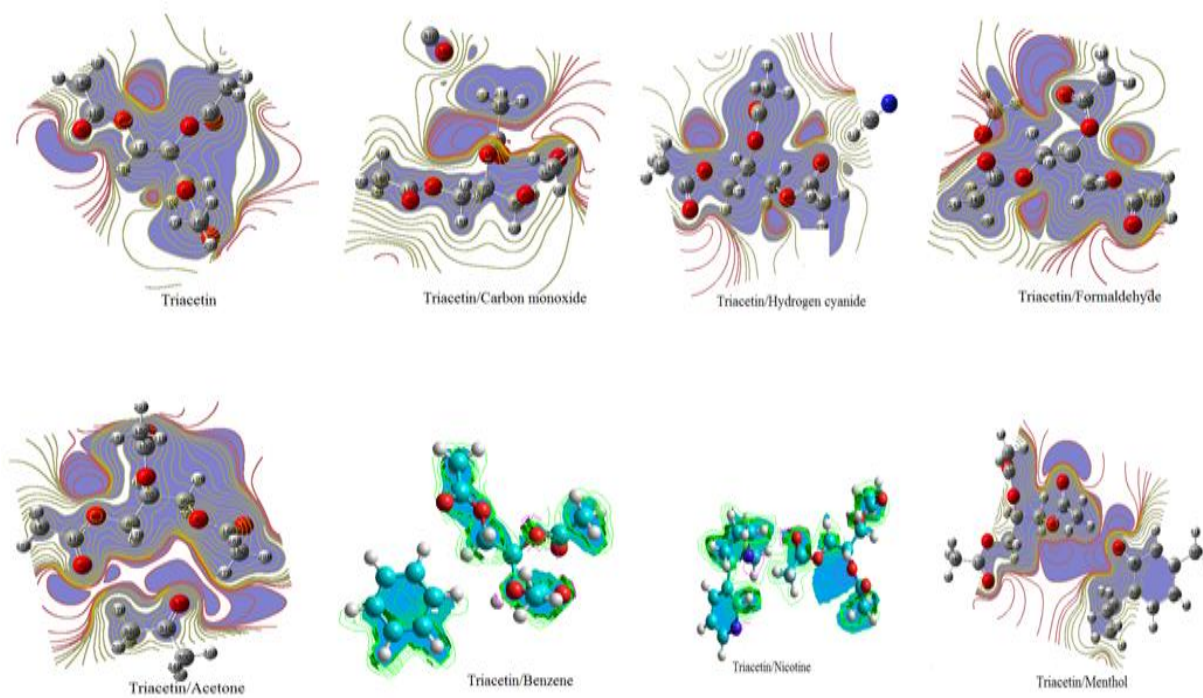


Figure 5 Electrostatic potential surface (ESP) contour map of triacetin and its complex with cigarette smoke chemical compounds in the gas phase.

Additionally, $V_b/G_b \leq 1$, indicating van der Waals interactions, which are weak. However, the bond

ellipticity for H40–O3 and H39–O5 is smaller than 0.1, whereas for the H39–H18 dihydrogen bond, it is significantly higher at 6.5 atomic units, exceeding 2.

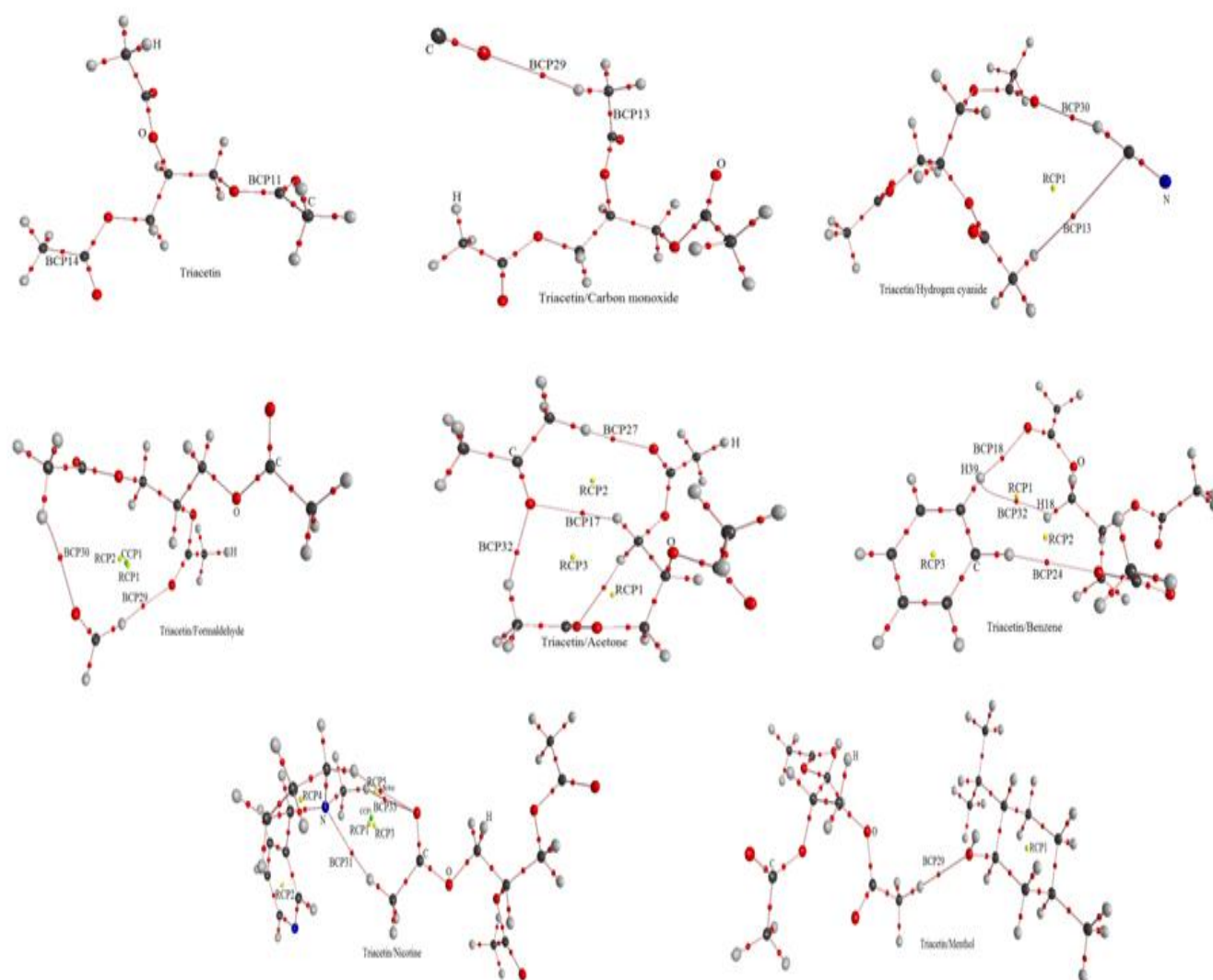


Figure 6 Molecular graph of the compound triacetin and its complexes with chemical compounds of cigarette smoke by QTAIM analysis in the gas phase (the bond critical point, ring critical point, cage critical point, and bond path are shown by red, yellow, green circles, and pink lines, respectively.)

The triacetin-nicotine complex features three intermolecular interactions involving the N40–H26, H52–O5, and H48–O5 bonds. These interactions are characterized by $\nabla^2\rho > 0$ and $H_b > 0$, the lowest charge density (ρ) among the bonds, $V_b/G_b \leq 1$, and bond ellipticity smaller than 0.1, confirming their van der Waals nature and weak strength. The triacetin-menthol complex contains one intermolecular interaction related to the H29–O30 bond. This interaction has $\nabla^2\rho > 0$ and $H_b > 0$, with the lowest charge density (ρ), $V_b/G_b \leq 1$, and bond ellipticity approximately 0.1, confirming its van der Waals character and weak interaction.

In Table 7, the number and types of critical points for the optimized structure of triacetin and its complexes, which reflect their topological properties, are presented using the Poincaré–Hopf relation [41]: $n - b + r - c = 1$. Here, n represents the number of core critical points (NCP), b the number of (BCP), r the number of (RCP), and c the number of (CCP). The Poincaré–Hopf relation defines the number and types of critical points in a system. The set of NCP, BCP, RCP and CCP ensures the topological stability of structures and complexes. This relation, by incorporating changes in electron distribution, provides detailed information about the bond nature, including its path and critical point [42].

According to the calculations in Table 7 and Figure 6, the Triacetin compound contains 28 (BCP). For the triacetin-carbon monoxide complex, there are 30 (BCPs). The triacetin-hydrogen cyanide complex contains 32 (BCPs) and 1 (RCP). The triacetin-formaldehyde complex features 33 (BCPs), 2 (RCPs) and 1 (CCP), where the cage critical point is enclosed by two ring critical points [43].

Mathematically, for compounds with cage critical points enclosed by only two ring critical points, the configuration is minimal. However, in real molecules, a cage critical point typically requires three ring critical points to form. The triacetin-acetone complex includes 41 (BCPs) and 3 (RCPs). The triacetin-benzene complex contains 43 (BCPs) and 3 (RCPs), with bond critical point 32 corresponding to a dihydrogen bond (H18–H39). The triacetin-nicotine complex comprises 58 (BCPs), 5 (RCPs), and 1 (CCP), with the cage critical point enclosed by three ring critical points (RCPs). The triacetin-menthol complex has 60 bond critical points (BCPs) and 1 ring critical point (RCP). The results in Table 7 confirm that the Poincaré–Hopf relationship is mathematically consistent for the triacetin structure and its complexes with cigarette smoke chemical compounds, ensuring a topologically stable set of critical points. Moreover, for these structures even slight geometric changes can eliminate other vibrations

Table 7 Molecular graph calculations for the optimized structure of triacetin and its complexes with seven chemical compounds present in mainstream cigarette smoke in the gas phase. Number of nuclear critical points (n_{NCP}), number of bond critical points (n_{BCP}), number of ring critical points (n_{RCP}), number of cage critical points (n_{CCP}).

System	Property			
	n_{NCP}	n_{BCP}	n_{RCP}	n_{CCP}
Triacetin	29	28	-	-
Triacetin/Carbon monoxide	31	30	-	-
Triacetin/Hydrogen cyanide	32	32	1	-
Triacetin/Formaldehyde	33	33	2	1
Triacetin/Acetone	39	41	3	-
Triacetin/Benzene	41	43	3	-
Triacetin/Nicotine	55	58	5	1
Triacetin/Menthol	60	60	1	-

4- Conclusion

This study investigates the physical adsorption and molecular interactions of triacetin, a key component in cigarette filters, with various chemical compounds in cigarette smoke using quantum mechanics and DFT calculations at the B3LYP/6-311++G** level. The analysis covers computational energy, thermodynamic parameters, electronic properties, and QTAIM studies. The triacetin-hydrogen cyanide complex demonstrates greater stability, with the strongest adsorption interaction observed in the O6-H31 bond measuring 2.02 Å. Electronic charge transfer analysis reveals that triacetin acts as an electron donor in hydrogen cyanide and benzene complexes, while serving as an electron acceptor in carbon monoxide, acetone, and menthol interactions. In formaldehyde and nicotine complexes, triacetin simultaneously donates and accepts electrons, facilitating adsorption. QTAIM results confirm covalent bonding within triacetin, while its interactions with cigarette smoke compounds involve closed-shell van der Waals forces. Novel topological features are identified, including cage critical points observed in the triacetin-formaldehyde complex, resembling polycyclic aromatic hydrocarbons, and dihydrogen bonding detected in the triacetin-benzene complex, confirmed through topological analysis. These findings enhance the understanding of triacetin's adsorption efficiency in cigarette filters, demonstrating its role in modifying the distribution and stability of smoke compounds. The discovery of cage critical points and dihydrogen bonding highlights non-classical interactions, contributing to potential advancements in cigarette filter design to reduce toxic emissions.

Acknowledgements

Authors are grateful to the of Tirtash Tobacco Research and Education center for financial support.

References

- [1] Kong, P. S.; Aroua, M. K.; Daud, W. M. A. W.; Lee, H. V.; Cognet, P.; Peres, Y. Catalytic role of solid acid catalysts in glycerol acetylation for the production of bio-additives: a review. *RSC Adv.* **2016**, 6(73), 68885–68905.
- [2] Bonet, J.; Costa, J.; Sire, R.; Reneaume, J.; Plesu, E. A.; Plesu, V.; Bozga, G. Revalorization of glycerol: Comestible oil from biodiesel synthesis. *Food Bioprod. Process* **2009**, 87, 171–178.
- [3] Fukumura, T.; Toda, T.; Seki, M.; Kubo, Y.; Kitakawa, N. S.; Yonemoto, T. Catalytic synthesis of glycerol monoacetate using a continuous expanded bed column reactor packed with cation-exchange resin. *Ind. Eng. Chem. Res.* **2009**, 48, 1816–182
- [4] Galan, M. I.; Bonet, J.; Sire, R.; Reneaume, J. M.; Plesu, A. E. From residual to use oil: revalorization of glycerine from biodiesel synthesis. *Bioresour. Technol.* **2009**, 100, 3775–3778.
- [5] Hou, J.; Zhang, Q.; Shi, W.; Li, Y. New process for synthesis of triacetin. *Henan Huagong* **1998**, 15, 18–19.
- [6] Luque, R. L.; Budarin, V.; Clark, J. H.; Macquarrie, D. J. Glycerol transformations on polysaccharide-derived mesoporous materials. *Appl. Catal. B Environ.* **2008**, 82, 157–162.
- [7] Missen, R. W.; Mims, C. A.; Saville, B. A. *Introduction to Chemical Reaction Engineering and Kinetics*; John Wiley and Sons: New York, **1999**.
- [8] Mufrodi, Z.; Rochmadi, S.; Sutijan, A.; Budiman, A. Effects of temperature and catalyst upon triacetin production from glycerol (by-product biodiesel production) as octane booster. *Proc. Adv. Renew. Energy Technol. Int. Conf.*, **2010**, Cyberjaya, Malaysia, 130–134.
- [9] Ranjbar, M.; Tadayon, M. R.; Tadayyon, A.; Ebrahimi, R. Effects of nitrogen, potassium, magnesium, and zinc sulfate fertilizers on the yield and some characteristics of biodiesel production in safflower. *New J. Crop Prod. Process.* **2012**, 2(4), 67–76.
- [10] Bonet, J.; Costa, J.; Sire, R.; Reneaume, I. M.; Plesu, U. A.; Plesu, U. V.; Bozga, G. Revalorization of glycerol: Comestible oil from biodiesel synthesis. *Food Bioprod. Process* **2009**, 87, 171–178.
- [11] Mohsen, S. M.; Ammar, A. S. M.; Ateya, A. F. Effect of cigarette filter components on its efficiency and smoking characteristics of cigarettes. *Biosci. Res.* **2018**, 15(1), 325–336.
- [12] Wilkinson, E.; Hoh, E.; Stack, M.; Mladenov, N.; Youssef, G. Thermal, physical, chemical, and mechanical properties of cellulose acetate from cigarette filters. *J. Appl. Polym. Sci.* **2025**, 142(22), 56946.
- [13] Robert, K. Tobacco smoke. *Encyclopedia of Toxicology*, **2005**, 4(2nd ed.), Elsevier, 200–202.
- [14] Tso, T. C. Tobacco. *Ullmann's Encyclopedia of Industrial Chemistry*, **2007**, (7th ed.), Wiley, 1–26.
- [15] Fiume, M. Z. Final report on the safety assessment of triacetin. *Int. J. Toxicol.* **2003**, 22(2), 1–10.

- [16] Hazen, R. M.; Trel, J. *Science Matters*; Anchor: New York, **1991**.
- [17] Hall, G. G. The growth of computational quantum chemistry from 1950 to 1971 *Chem. Soc. Rev.* **1973**, *2*, 21-28.
- [18] Lichtenstein, A. I.; Zaanen, J.; Anisimov, V. I. Density-functional theory and strong interactions: Orbital ordering in Mott-Hubbard insulators. *Phys. Rev. B* **1995**, *52*, R5467.
- [19] Glendening, E. D.; Reed, A. E.; Carpenter, J. A.; Weinhold, F. NBO Version 3.1.
- [20] Dennington, R.; Keith, T.; Millam, J. *GaussView 5.0*; Semichem Inc.: Shawnee Mission, KS, **2009**.
- [21] Becke, A. D. Density-functional thermochemistry. III. The role of exact exchange *J. Chem. Phys.* **1993**, *98*, 5648-5652.
- [22] Frisch, M. J.; et al. *Gaussian 09, Revision A.2*; Gaussian, Inc.: Wallingford, CT, **2009**.
- [23] Bader, R. F. *Atoms in Molecules: A Quantum Theory*; Oxford University Press: Oxford, UK, **1990**.
- [24] Biegler-König, F.; Schönbohm, J.; Bayles, D. AIM-2000: A program to analyze and visualize atoms in molecules. *J. Comput. Chem.* **2001**, *22*, 454-559.
- [25] Mayor-Lopez, M. J.; Weber, J. DFT calculations of the binding energy of metallocenes. *Chem. Phys. Lett.* **1997**, *281*, 226-232.
- [26] van Duijneveldt, F. B. V. State of the art in counterpoise theory. *Chem. Rev.* **1994**, *94*, 1873-1885.
- [27] Senent, M. L.; Wilson, S. Intramolecular basis set superposition errors. *Int. J. Quantum Chem.* **2001**, *82*, 282-292.
- [28] Jensen, F. *Introduction to Computational Chemistry*; John Wiley & Sons: 3rd ed.; ISBN: 978-1-118-82599-0, **2017**.
- [29] Reed, A. E.; Curtiss, L. A.; Weinhold, F. Intermolecular interactions from a natural bond orbital, donor-acceptor viewpoint. *Chem. Rev.* **1988**, *88*, 899-926.
- [30] Gutowski, M.; Lenthe, J. H. V.; Duijneveldt, F. B. V. Accuracy of the Boys and Bernardi function counterpoise method. *J. Chem. Phys.* **1993**, *98*, 4728-4738.
- [31] Yang, C.; Wang, H. Ab initio and DFT theory studies of interaction of thymine with formaldehyde. *Struct. Chem.* **2008**, *19*, 843-847.
- [32] Ardalan, P.; Ardalan, T.; Momen, M.; Heravi, J. A DFT Study on Antioxidant Activity of Trolox and Substituted Trolox and Their Radicals *J. Appl. Chem.* **2014**, *8*, 45-50.
- [33] Chattaraj, P. K.; Poddar, A. Chemical reactivity and excited-state density functional theory. *J. Phys. Chem. A* **1999**, *103*, 8691.
- [34] Parr, R. G.; Szentpaly, L. V.; Liu, S. Electrophilicity Index. *Journal of the American Chemical Society*, *121*, 1922-1924. *J. Am. Chem. Soc.* **1999**, *121*, 1922-1924.
- [35] Pyykkö, P. Spectroscopic nuclear quadrupole moments *Mol. Phys.* **2001**, *99*, 1617-1529.
- [36] Baei, M. T.; Moghimi, M.; Torabi, P.; Varasteh Moradi, A. Adsorption properties of N2O on (6,0), (7,0), and (8,0) zigzag single-walled boron nitride nanotubes: a computational study *Comput. Theor. Chem.* **2011**, *970*(1), 30-35.
- [37] Shariatnia, Z.; Shahidi, S. A DFT study on the physical adsorption of cyclophosphamide derivatives on the surface of fullerene C60 nanocage *J. Mol. Graph. Model.* **2014**, *52*, 71-81.
- [38] Iwaoka, M.; Komatsu, H.; Katsuda, T.; Tomoda, S. Nature of Nonbonded Se...O Interactions Characterized by ¹⁷O NMR Spectroscopy and NBO and AIM Analyses *J. Am. Chem. Soc.* **2004**, *126*, 5309-5317.
- [39] Bader, R. F. W.; Essen, H. The characterization of atomic interactions. *J. Chem. Phys.* **1984**, *80*, 1943-1960.
- [40] Bone, R. G. A.; Bader, R. F. W. Identifying and Analyzing Intermolecular Bonding Interactions in van der Waals Molecules. *J. Phys. Chem.* **1996**, *100*, 10892-10911.
- [41] Bader, R. F. W. *Atoms in Molecules: A Quantum Theory*; Oxford University Press: USA, **1994**, p. 458.
- [42] Popelier, P. L. A. *Atoms in Molecules: An Introduction*; Prentice-Hall: London, **2000**.
- [43] Castillo, N.; Matta, C. F.; Boyd, R. J. The first example of a cage critical point in a single ring: A novel twisted α -helical ring topology. *Chem. Phys. Lett.* **2005**, *409*(4-6), 265-269.